



MODELLING THE TOPOLOGICAL FEATURES OF EXOTIC SEMIMETALS

Written by *John E. Montgomery*
June 13, 2018

Supervised by
Michele Burrello

UNIVERSITY OF COPENHAGEN

An abstract geometric diagram consisting of several overlapping circles and lines, forming a complex shape that resembles a stylized letter 'C' or a similar symbol. The diagram is rendered in thin black lines on a white background.



UNIVERSITY OF
COPENHAGEN

NAME OF INSTITUTE: Niels Bohr Institute

NAME OF DEPARTMENT: Condensed Matter Theory

AUTHOR(S): John E. Montgomery

EMAIL: sbf253@alumni.ku.dk

TITLE AND SUBTITLE: Modelling the topological features of exotic semimetals

-

SUPERVISOR(S): Michele Burrello

HANDED IN: 12.6.2018

DEFENDED: 2.7.2018

NAME _____

SIGNATURE _____

DATE _____

Abstract

I study the Weyl semimetal and TPC semimetal near their topological charge monopoles with the goal of finding an analytical description of the surface states characteristic of topological semimetals, for the TPC (triple point crossing). I derive a k-space bulk Hamiltonian for a system and demonstrate that it hosts TPC's. I examine the constraint of self-adjointness on a Weyl or TPC system, with a physical boundary and what restriction that places on the surface states. Finally I compare my derived surface states to a numerical simulation of the TPC semimetal I am examining.

Contents

1	Introduction	1
2	TPC Hamiltonian derived from real-space lattice	3
3	Boundary Conditions on Weyl equation	8
3.1	Probability current density for Weyl Hamiltonian	10
4	Boundary condition in linearized TPC	10
5	Deriving surface states	13
6	BZ Analytics comparison to data using amplitude approach	15
7	Analytical wavefunctions compared to data	17
8	Conclusion	19
A	Appendix	22
A.1	Berry curvature monopoles of the Weyl Hamiltonian	22

1 Introduction

In modern physics, the correspondence between high energy relativistic particle physics and low energy condensed matter physics has historically been a source of much insight. Particles predicted from the relativistic Dirac equation, like the Dirac fermion, have seen equivalent quasiparticles in condensed matter physics, graphene being the most known example. While there are definitely no elementary Dirac fermions in graphene, the periodic crystal potential, that graphene imposes upon its resident electrons, gives way to quasiparticles with the properties of relativistic Dirac fermions albeit at a much lower velocity.

The Dirac equation was proposed in 1928 by Paul Dirac and became the basis for the unification of quantum mechanics and special relativity [1]. One year later, in 1929, Hermann Weyl pointed out that by removing mass from the Dirac equation, one can make a simpler Weyl equation that describes massless fermions with definite chirality [2]. In 1937 Ettore Majorana found a modification on the Dirac equation that allowed for another class of fermions based on the Majorana equation. These fermions would have the unique property of being their own antiparticle.

The three solutions to the Dirac equation give rise to three different kinds of fermionic particles: Dirac fermions, Weyl fermions and Majorana fermions. While the Dirac equation has had much success in describing relativistic electrons and the Majorana equation is a candidate for the description of the neutrino, the Weyl equation has stood without experimental candidates for Weyl fermions in high energy physics for 89 years.

In 1937 Conyers Herring [3], while studying degeneracies of electron bands, found that in the absence of any particular symmetry one could have a degeneracy in energy of electron bands at the same crystal momentum. The particles emergent at these crossing points were described by the Weyl equation. In modern times these crossing points have been dubbed Weyl nodes.

When tracing the wavefunction of an electron around a magnetic monopole in real space, creating a closed loop, one finds that it acquires a phase. This same phenomenon happens when one traces a loop around a Weyl node in k -space for a many body wavefunction in condensed matter physics. The Weyl nodes thus serve as equivalents to sources of magnetic charge but in k -space. Instead of charges they are topological charges, monopoles of Berry curvature or Berry flux [4]. See Appendix A for an explicit calculation of this.

As mentioned previously, Weyl fermions have definite chirality. This chirality is equivalent to the topological charge of the Weyl nodes which the Weyl fermions are excitations of and it is quantized. The Nielsen–Ninomiya theorem states that the monopoles of Berry curvature must always come in pairs [5]. The net topological charge of Berry curvature over the entire Brillouin zone must be equal to zero. It can be shown that if this is not the case, electric charge is not conserved in the presence of parallel electric and magnetic fields [6]. A minimum of two Weyl nodes are therefore always present in a system that hosts Weyl fermion quasiparticles [7, 8].

Because of the conservation of Berry monopole charge, the Weyl nodes are extremely resilient to imperfections in the host crystal or small perturbations. As long as transla-

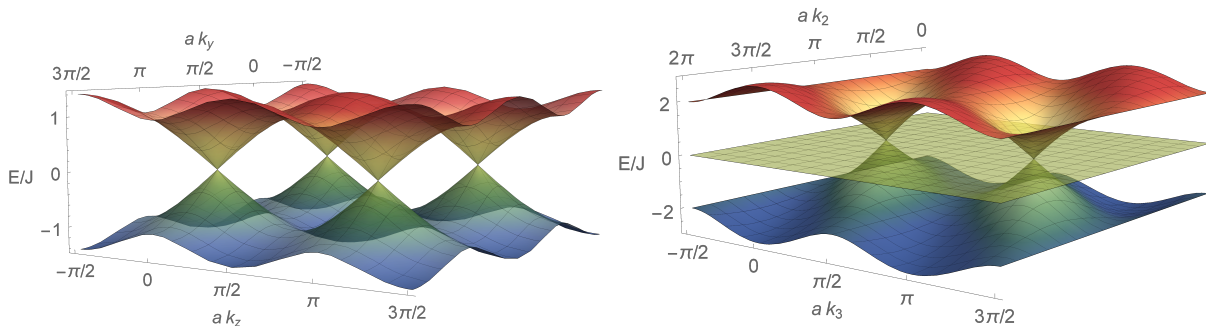


Figure 1: *Left: Plot of dispersion relation of equation 1.1 with $k_1 = \pi$. This is an example of a system with Weyl nodes. Right: Dispersion relation plot of equation 2.20. The TPC system examined throughout the thesis.*

tional invariance is not broken, the Weyl nodes will continue to exist regardless of small perturbations. It is possible to remove Weyl nodes from a system by introducing a large enough perturbation that does not break translational invariance. Doing so would continuously move the Weyl nodes towards each other in k -space until they occupy the same point, at which point a gap would open in the bands and the system would become an insulator [9, 10].

Semimetals are a category of systems, that in band theory have multiple bands, but at a given Fermi energy have multiple partially filled bands, typically displaying small Fermi surfaces. In the most extreme cases, the Fermi surface can shrink to a discrete set of points. Topological semimetals are semimetals that have Weyl nodes at the Fermi energy, or higher monopole generalizations of them. The simplest topological semimetal is the Weyl semimetal, given by the Weyl equation close to the Fermi energy $H_{weyl} = \vec{\sigma} \cdot \vec{k}$, where $\vec{\sigma}$ is the vector of Pauli spin matrices and \vec{k} is the momentum vector [10, 11]. An example of such a system could be:

$$H_{weyl} = J(\sigma_x \sin(k_x) + \sigma_y \sin(k_y) + \sigma_z \sin(k_z)) \quad (1.1)$$

Near the Fermi energy at $(k_1, k_2, k_3) = (0, 0, 0)$ this becomes the Weyl equation.

$$H_{weyl} \approx J(\sigma_x k_x + \sigma_y k_y + \sigma_z k_z) = J\vec{\sigma} \cdot \vec{k} \quad (1.2)$$

The dispersion relation can be seen in full on figure 1.

A more complicated system with higher monopoles of the Berry curvature present the so called triple points crossing (TPC), sometimes referred to as triple point fermions. This system has three bands instead of two, and has the following dispersion relation near the Fermi surface $H_{TPC} = \vec{S} \cdot \vec{k}$ [12], where \vec{S} is the vector of the three 3×3 matrices $(S_j)_{kl} = -i\epsilon_{jkl}$, which are the three generators of rotation in $SO(3)$. This dispersion relation can be seen on figure 1 and features two bands that are linear near the Berry curvature monopole, hence known as the TPC and one flat band. The TPC is less stable than the Weyl node and requires additional chiral symmetries whose analysis is beyond the scope of this thesis [13, 14]. The monopoles of the TPC have chirality ± 2 instead of the ± 1 of the Weyl nodes [14, 12].

It has been shown that only a finite number of zero gap topological semimetals exist, that are protected by lattice symmetries [12]. This makes the cataloging of their properties all the more interesting. The TPC is one of these semimetals.

A property characteristic of topological semimetals like the TPC and the Weyl semimetal is a linear dispersion relation near their Berry flux monopole. Similar to 2D topological materials, one of the main characteristics of these topological systems is the appearance of chiral surface modes with Fermi-arcs, that continuously exist between the monopoles in k -space when a boundary is introduced [4, 15]. The states that form these Fermi-arcs are localized surface states, localized on the boundaries of the system. This is a property of Weyl fermions unique to condensed matter physics and has no parallel in high energy physics.

The aim of this thesis is to explore and derive an analytical description of surface states in a TPC system, once a boundary is introduced into the system. The main tool I will exploit is the self-adjoint extensions of the Hamiltonians, describing the TPC semimetals. While the bulk Hamiltonian is self-adjoint and Hermitian upon a Hilbert space that spans all of \mathbb{R}^3 and has no boundaries, that may not necessarily be true for the same system but restricted to a slab with finite length in one dimension. One must limit oneself to a domain (of the Hilbert space) upon which the Hamiltonian is self-adjoint with the boundary [16]. This requirement vastly limits the form of wavefunctions that can exist.

2 TPC Hamiltonian derived from real-space lattice

The system I am working with is a 3-D Lieb lattice as described in [14]. The Lieb lattice is a 2-D structure made out of L shaped unit cells with 3 sites. The unit cell that defines it is as follows: Site 1 is located at $(1,0)$, site 2 is located at $(0,0)$ and site 3 is located at $(0,1)$, with Bravais lattice vectors $a_1 = (2,0)$ and $a_2 = (0,2)$, as seen on figure 2, using units where the lattice spacing in the square lattice is $a = 1$.

To expand this to 3-D we extend the lattice along a third direction with Bravais vector $a_3 = (1,1,1)$, changing $a_1 = (2,0,0)$ and $a_2 = (0,2,0)$. Keeping 3 sites within the unit cell with the basis: site 1 = $(1,0,0)$, site 2 = $(0,0,0)$ and site 3 = $(0,1,0)$. This creates the unit cell seen on figure 3 in green. It is created such that any 2-D plane cut along any of the Cartesian axes will form a Lieb lattice. Thus there is no favored axis with the addition of the third dimension.

The reciprocal lattice vectors $\hat{k}_1, \hat{k}_2, \hat{k}_3$ are the following:

$$\begin{pmatrix} a_1 = (2, 0, 0) \\ a_2 = (0, 2, 0) \\ a_3 = (1, 1, 1) \end{pmatrix} \quad \begin{matrix} \hat{k}_1 = (1/2, 0, -1/2) \\ \hat{k}_2 = (0, 1/2, -1/2) \\ \hat{k}_3 = (0, 0, 1) \end{matrix} \quad (2.1)$$

Considering only nearest neighbor coupling where $C_{\vec{r}}$ is the fermionic annihilation operator at the site located at \vec{r} and $C_{\vec{r}}^\dagger$ is the creation operator, yields a real space Hamiltonian

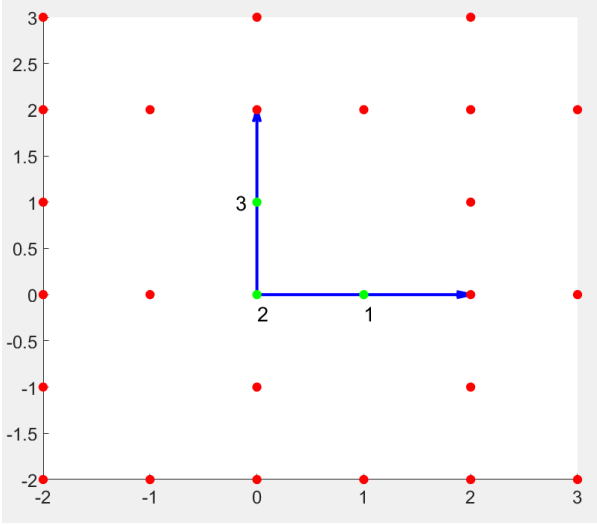


Figure 2: *The Lieb lattice. A unit cell is shown in green with blue arrows being the Bravais lattice vectors.*

that reads [14]:

$$H = -J \left(\sum_{\vec{r}, (-1)^{x+y}=-1} C_{\vec{r}+\vec{z}}^\dagger C_{\vec{r}} + \sum_{\vec{r}, (-1)^{x+z}=-1} C_{\vec{r}+\vec{y}}^\dagger C_{\vec{r}} + \sum_{\vec{r}, (-1)^{y+z}=-1} C_{\vec{r}+\vec{x}}^\dagger C_{\vec{r}} \right) + h.c. \quad (2.2)$$

where the boolean requirement in the sums require 2-sites to couple in the x-y plane, 3-sites to couple in the y-z plane and 1-sites to couple in the x-z plane. I introduce a vector potential \vec{A} which applies a phase to every coupling[17, 18, 19], based on the direction of the coupling as shown below in equation 2.3.

$$C_{\vec{r}+\vec{n}}^\dagger C_{\vec{r}} \rightarrow e^{i \int_{\vec{r}}^{\vec{r}+\vec{n}} \vec{A} \cdot d\vec{l}} C_{\vec{r}+\vec{n}}^\dagger C_{\vec{r}} \quad (2.3)$$

By taking $\vec{A} = \pi \left(0, 0, x - z + \frac{1}{2} \right)$ we get the following phase change in the z-direction[14].

$$H = -J \left(\sum_{\vec{r}, (-1)^{x+y}=-1} (-1)^{x-z} C_{\vec{r}+\vec{z}}^\dagger C_{\vec{r}} + \sum_{\vec{r}, (-1)^{x+z}=-1} C_{\vec{r}+\vec{y}}^\dagger C_{\vec{r}} + \sum_{\vec{r}, (-1)^{y+z}=-1} C_{\vec{r}+\vec{x}}^\dagger C_{\vec{r}} \right) + h.c. \quad (2.4)$$

Introducing a notation where the creation and annihilation operators have 4 indices: The first index is the site number within the unit cell and the next 3 indicate the coordinate in terms of the Bravais vectors.

$$C_{\text{site}, l, m, n}^\dagger \quad (2.5)$$

The Hamiltonian can now be written as a sum using only the indices l, m, n specifying the unit cell.

$$H = H_{xy} + H_z \quad (2.6)$$

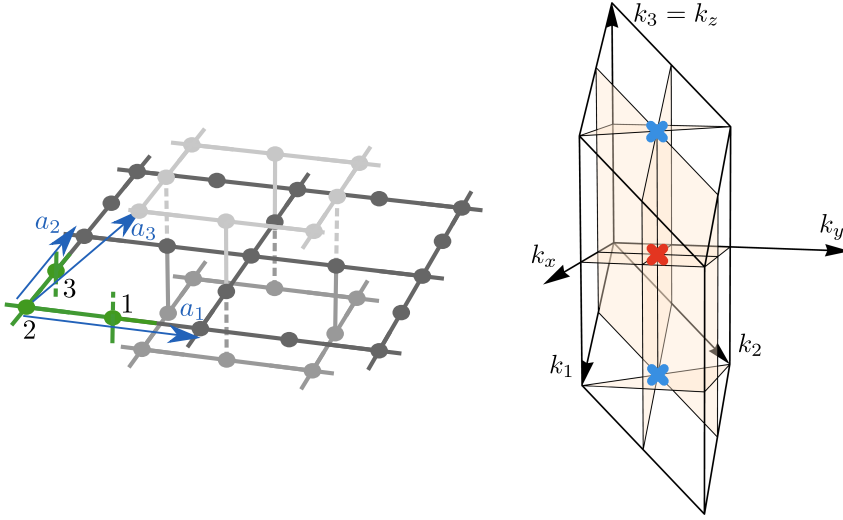


Figure 3: The figure to the left shows the 3-D Lieb lattice. The sites are numerated based on their lattice vectors; solid lines have normal tightbinding coupling while dashed lines have a negative sign due to the applied vector potential. The right side shows the Brillouin zone and the reciprocal lattice vectors inside of it. The blue and red points are the two Weyl points where the three bands touch. Picture taken from [14]

where H_{xy} includes all the terms for hopping in the x-y plane and H_z includes the hopping terms that change z-coordinate.

$$H_{xy} = -J \sum_{l,m,n} C_{1,l,m,n}^\dagger C_{2,l,m,n} + C_{3,l,m,n}^\dagger C_{2,l,m,n} + C_{1,l-1,m,n}^\dagger C_{2,l,m,n} + C_{3,l,m-1,n}^\dagger C_{2,l,m,n} + h.c \quad (2.7)$$

$$H_z = -J \sum_{l,m,n} C_{1,l-1,m,n+1}^\dagger C_{3,l,m,n} + C_{3,l+1,m,n-1}^\dagger C_{1,l,m,n} - J \sum_{l,m,n} -C_{1,l,m+1,n-1}^\dagger C_{3,l,m,n} - C_{3,l,m-1,n+1}^\dagger C_{1,l,m,n} \quad (2.8)$$

I use the Fourier transform of the annihilation and creation operators to transform the Hamiltonian into k-space, where k_i labels the momentum coordinate along \hat{k}_i [18].

$$C_{\text{site},l,m,n} = \frac{1}{\sqrt{V}} \int_{-\infty}^{\infty} d\vec{k} e^{-i(k_1 l + k_2 m + k_3 n)} C_{\text{site}}(\vec{k}) \quad (2.9)$$

I further subdivide H_{xy} into terms that couple sites 1 and 2, and terms that couple sites 3 and 2. Since $H_{1,2}$ and $H_{3,2}$ are identical in form, due to the symmetry between x and y direction in our system, I only need to evaluate one of the terms.

$$H_{xy} = -J \sum_{l,m,n} \underbrace{C_{1,l,m,n}^\dagger C_{2,l,m,n}}_{H_{1,2,in}} + \underbrace{C_{3,l,m,n}^\dagger C_{2,l,m,n}}_{H_{3,2,in}} + \underbrace{C_{1,l-1,m,n}^\dagger C_{2,l,m,n}}_{H_{1,2,out}} + \underbrace{C_{3,l,m-1,n}^\dagger C_{2,l,m,n}}_{H_{3,2,out}} + h.c \quad (2.10)$$

I split $H_{1,2}$ in two parts: The part that has coupling inside the unit cell.

$$\begin{aligned}
 H_{1,2,in} &= -J \sum_{l,m,n} \frac{1}{V} \int_{-\infty}^{\infty} \int_{-\infty}^{\infty} d\vec{k} d\vec{k}' e^{i(k_1 l + k_2 m + k_3 n)} C_1^\dagger(\vec{k}) e^{-i(k'_1 l + k'_2 m + k'_3 n)} C_2(\vec{k}') + h.c \\
 &= -J \frac{1}{V} \int_{-\infty}^{\infty} \int_{-\infty}^{\infty} d\vec{k} d\vec{k}' \underbrace{\sum_{l,m,n} e^{i((k_1 - k'_1)l + (k_2 - k'_2)m + (k_3 - k'_3)n)}}_{V\delta(\vec{k} - \vec{k}')} C_1^\dagger(\vec{k}) C_2(\vec{k}') + h.c \\
 &= -J \sum_{\vec{k}} C_1^\dagger(\vec{k}) C_2(\vec{k}) + h.c
 \end{aligned} \tag{2.11}$$

And the part that has coupling outside the unit cell.

$$\begin{aligned}
 H_{1,2,out} &= -J \sum_{l,m,n} C_{1,l-1,m,n}^\dagger C_{2,l,m,n} + h.c. \\
 &= -J \frac{1}{V} \sum_{l,m,n} \int_{-\infty}^{\infty} \int_{-\infty}^{\infty} d\vec{k} d\vec{k}' e^{i((k_1 - k'_1)l + (k_2 - k'_2)m + (k_3 - k'_3)n)} C_{1,l-1}^\dagger(\vec{k}) C_2(\vec{k}') e^{-ik_1} + h.c \\
 &= -J \sum_{\vec{k}} C_{1,l-1}^\dagger(\vec{k}) C_2(\vec{k}) e^{-ik_1} + h.c
 \end{aligned} \tag{2.12}$$

Combining the above I get $H_{1,2}$ and $H_{3,2}$.

$$H_{1,2} = -J \sum_{\vec{k}} C_1^\dagger(\vec{k}) C_2(\vec{k}) (1 + e^{-ik_1}) \tag{2.13}$$

$$H_{2,3} = -J \sum_{\vec{k}} C_3^\dagger(\vec{k}) C_2(\vec{k}) (1 + e^{-ik_2}) \tag{2.14}$$

I move on to solve H_z

$$\begin{aligned}
 H_z &= -J \sum_{l,m,n} \underbrace{C_{1,l-1,m,n+1}^\dagger C_{3,l,m,n} + C_{3,l+1,m,n-1}^\dagger C_{1,l,m,n}}_{H_{z,+}} \\
 &\quad \underbrace{-C_{1,l,m+1,n-1}^\dagger C_{3,l,m,n} - C_{3,l,m-1,n+1}^\dagger C_{1,l,m,n}}_{H_{z,-}}
 \end{aligned} \tag{2.15}$$

Focusing only on the parts where site 1 is created.

$$\begin{aligned}
 H_{z,1,3+} &= -J \sum_{l,m,n} C_{1,l-1,m,n+1}^\dagger C_{3,l,m,n} \\
 &= -J \frac{1}{V} \int_{-\infty}^{\infty} \int_{-\infty}^{\infty} d\vec{k} d\vec{k}' \sum_{l,m,n} e^{i((k_1 - k'_1)l + (k_2 - k'_2)m + (k_3 - k'_3)n)} C_{1,l-1}^\dagger(\vec{k}) C_3(\vec{k}') e^{i(-k_1 + k_3)} \\
 &= -J \sum_{\vec{k}} C_{1,l-1}^\dagger(\vec{k}) C_3(\vec{k}') e^{i(-k_1 + k_3)}
 \end{aligned}$$

$$(2.16)$$

Subdividing further into terms that acquire a negative sign because of the vector potential \vec{A} and the ones having a positive sign.

$$\begin{aligned} H_{z,1,3-} &= J \sum_{l,m,n} C_{1,l,m+1,n-1}^\dagger C_{3,l,m,n} \\ &= -J \frac{-1}{V} \int_{-\infty}^{\infty} \int_{-\infty}^{\infty} d\vec{k} d\vec{k}' \sum_{l,m,n} e^{i((k_1-k'_1)l+(k_2-k'_2)m+(k_3-k'_3)n)} C_{1,1}^\dagger(\vec{k}) C_3(\vec{k}') e^{i(k_2-k_3)} \\ &= J \sum_{\vec{k}} C_{1,1}^\dagger(\vec{k}) C_3(\vec{k}) e^{i(k_2-k_3)} \end{aligned} \quad (2.17)$$

I combine it and get the following H_z

$$H_z = -J \sum_{\vec{k}} C_{1,1}^\dagger(\vec{k}) C_3(\vec{k}) (e^{i(-k_1+k_3)} - e^{i(k_2-k_3)}) + h.c \quad (2.18)$$

Giving me the following complete Hamiltonian

$$\begin{aligned} H &= H_z + H_{1,2} + H_{3,2} \\ &= -J \begin{pmatrix} C_{1,1}^\dagger & C_{1,2}^\dagger & C_{1,3}^\dagger \end{pmatrix} \begin{pmatrix} 0 & 1 + e^{-ik_1} & e^{-i(-k_3+k_1)} - e^{-i(k_3-k_2)} \\ 1 + e^{ik_1} & 0 & 1 + e^{ik_2} \\ e^{i(-k_3+k_1)} - e^{i(k_3-k_2)} & 1 + e^{-ik_2} & 0 \end{pmatrix} \begin{pmatrix} C_1 \\ C_2 \\ C_3 \end{pmatrix} \end{aligned} \quad (2.19)$$

The bulk Hamiltonian in k-space is then the following: [14].

$$H = -J \begin{pmatrix} 0 & 1 + e^{-ik_1} & e^{-i(-k_3+k_1)} - e^{-i(k_3-k_2)} \\ 1 + e^{ik_1} & 0 & 1 + e^{ik_2} \\ e^{i(-k_3+k_1)} - e^{i(k_3-k_2)} & 1 + e^{-ik_2} & 0 \end{pmatrix} \quad (2.20)$$

with 0-point energy at $(k_1, k_2, k_3) = (\pi, \pi, \pi/0)$ and every multiple of 2π in any direction, as the Brillouin zone is periodic with 2π . The dispersion relation can be seen on figure 1. I wish to find the surface states that exist in this system when it is restrained by a wall at $x_1 = 0$, such that for $x_1 < 0$ the wavefunction vanishes. x_2 and x_3 are not restrained and go to minus and plus infinite. To make the problem simpler I do an expansion in k_1 around the 0 point for the Hamiltonian at $k_1 = \pi$.

$$H = J \begin{pmatrix} 0 & -i(k_1 - \pi) & e^{-k_3} + e^{-i(k_3-k_2)} \\ i(k_1 - \pi) & 0 & -1 - e^{ik_2} \\ e^{-ik_3} + e^{ik_3-k_2} & -1 - e^{-ik_2} & 0 \end{pmatrix} = J \begin{pmatrix} 0 & -\partial_{x_1} & \mu^\dagger \\ \partial_{x_1} & 0 & C^\dagger \\ \mu & C & 0 \end{pmatrix} \quad (2.21)$$

In the second equality I translate the Brillouin zone by π along k_1 and I have defined C and μ as the following:

$$\begin{aligned} \mu &= e^{-ik_3} + e^{ik_3-k_2} \\ C &= -1 - e^{-ik_2} \end{aligned}$$

To verify that my Hamiltonian does indeed describe a $H = \vec{S} \cdot \vec{k}$ TPC semimetal, I can simplify the problem by writing the Hamiltonian of equation 2.20 in Cartesian momenta space and expanding around the triple point crossing to first order. I use the following identity to map the momenta from the reciprocal lattice to Cartesian coordinates.

$$\vec{k} = k_1 \begin{pmatrix} 1/2 \\ 0 \\ -1/2 \end{pmatrix} + k_2 \begin{pmatrix} 0 \\ 1/2 \\ -1/2 \end{pmatrix} + k_3 \begin{pmatrix} 0 \\ 0 \\ 1 \end{pmatrix} = k_x \begin{pmatrix} 1 \\ 0 \\ 0 \end{pmatrix} + k_y \begin{pmatrix} 0 \\ 1 \\ 0 \end{pmatrix} + k_z \begin{pmatrix} 0 \\ 0 \\ 1 \end{pmatrix} \quad (2.22)$$

which results in:

$$k_1 = 2k_x \quad k_2 = 2k_y \quad k_3 = k_z + k_y + k_x \quad (2.23)$$

Mapping equation 2.20 into equation 2.24.

$$H = -J \begin{pmatrix} 0 & 1 + e^{-2ik_x} & e^{-i(k_x - k_y - k_z)} - e^{-i(-k_y + k_x + k_z)} \\ 1 + e^{2ik_x} & 0 & 1 + e^{2ik_y} \\ e^{i(k_x - k_y - k_z)} - e^{i(-k_y + k_x + k_z)} & 1 + e^{-2ik_y} & 0 \end{pmatrix} \quad (2.24)$$

In these coordinates the TPC is at $(k_x, k_y, k_z) = (\frac{\pi}{2}, \frac{\pi}{2}, 0)$ or $(k_x, k_y, k_z) = (\frac{\pi}{2}, \frac{\pi}{2}, \pi)$. I expand around the first of these TPC to linear order in \vec{k} .

Translating k_x and k_y into $k'_x = k_x - \frac{\pi}{2}$ and $k'_y = k_y - \frac{\pi}{2}$.

$$\frac{1}{2}H = -J \begin{pmatrix} 0 & ik'_x & -ik_z \\ -ik'_x & 0 & -ik'_y \\ ik_z & ik'_y & 0 \end{pmatrix} = -J \begin{pmatrix} 0 & \partial_x & -\partial_z \\ -\partial_x & 0 & -\partial_y \\ \partial_z & \partial_y & 0 \end{pmatrix} \quad (2.25)$$

Giving me the desired $H = \vec{S} \cdot \vec{k}$ expression up to a sign in the k_y and k_z direction, showcasing that the chosen system gives rise to TPC's in k-space.

3 Boundary Conditions on Weyl equation

Before addressing the problem of boundary conditions on the TPC, I wish to first examine the simplest semi-metal, the Weyl semimetal, and derive the maximal subspace of the Hilbert space that the Weyl Hamiltonian is self-adjoint within $(D(Q))$, specifically the condition 3.2. I start with the Weyl equation in the bulk. [10]

$$H = \vec{k} \cdot \vec{\sigma} = \begin{pmatrix} k_z & k_x - ik_y \\ k_x + ik_y & -k_z \end{pmatrix} \quad (3.1)$$

Bounding the wavefunction with $\psi = 0$ for $x < 0$, but making space infinite in y and z , such that k_y and k_z remain good quantum numbers and k_x does not, thus I substitute the momentum k_x with the differential operator $k_x = -i\partial_x$. I create the integral required

by the equation of self-adjointness.

$$\begin{aligned}
 & \langle H\psi|\phi\rangle - \langle\psi|H\phi\rangle = 0 \\
 & = \int_{-\infty}^{\infty} \int_{-\infty}^{\infty} \int_0^{\infty} dx dy dz \left(\begin{pmatrix} k_z & -i\partial_x - ik_y \\ -i\partial_x + ik_y & -k_z \end{pmatrix} \begin{pmatrix} \psi_1 \\ \psi_2 \end{pmatrix} \right)^\dagger \begin{pmatrix} \phi_1 \\ \phi_2 \end{pmatrix} \\
 & - \begin{pmatrix} \psi_1 \\ \psi_2 \end{pmatrix}^\dagger \begin{pmatrix} k_z & -i\partial_x - ik_y \\ -i\partial_x + ik_y & -k_z \end{pmatrix} \begin{pmatrix} \phi_1 \\ \phi_2 \end{pmatrix}
 \end{aligned} \tag{3.2}$$

Expanding the expression

$$\begin{aligned}
 & = \int_{-\infty}^{\infty} \int_{-\infty}^{\infty} \int_0^{\infty} dx dy dz \begin{pmatrix} k_z\psi_1 - i\partial_x\psi_2 - ik_y\psi_2 \\ -i\partial_x\psi_1 + ik_y\psi_1 - k_z\psi_2 \end{pmatrix}^\dagger \begin{pmatrix} \phi_1 \\ \phi_2 \end{pmatrix} \\
 & - \begin{pmatrix} \psi_1 \\ \psi_2 \end{pmatrix}^\dagger \begin{pmatrix} k_z\phi_1 - i\partial_x\phi_2 - ik_y\phi_2 \\ -i\partial_x\phi_1 + ik_y\phi_1 - k_z\phi_2 \end{pmatrix}
 \end{aligned}$$

All the terms that do not contain differentials of x cancel out and I am left with

$$0 = \int_{-\infty}^{\infty} \int_{-\infty}^{\infty} \int_0^{\infty} dx dy dz (i\partial_x\psi_2^\dagger\phi_1 + i\partial_x\psi_1^\dagger\phi_2 + i\psi_1^\dagger\partial_x\phi_2 + i\psi_2^\dagger\partial_x\phi_1)$$

Performing partial integration I am left only with the surface term created by the barrier at $x = 0$. Writing ψ instead of $\psi|_{x=0}$, meaning the wavefunction at the surface $x = 0$.

$$0 = [\psi_1^\dagger\phi_2 + \psi_2^\dagger\phi_1]_{x=0}^{x=\infty} = \langle\psi|\sigma_x|\phi\rangle \quad \sigma_x = \begin{pmatrix} 0 & 1 \\ 1 & 0 \end{pmatrix} \tag{3.3}$$

I now look for the space of wavefunctions at the surface of the system that conform to this equation, starting with the general normalized 2-vector. Taking $\theta \in [0, 2\pi]$ and $\chi \in [0, \pi]$.

$$\psi_j = \begin{pmatrix} \cos(\theta) \\ \sin(\theta) e^{i\chi} \end{pmatrix} \tag{3.4}$$

Any set of vectors inside the domain $D(Q)$, where the Hamiltonian is self-adjoint with my erected boundary must fulfill this equation, including the case where $\psi = \phi$. I thus choose the set of vectors where the parameters are the same.

$$\langle\psi_j|Q|\psi_j\rangle = \begin{pmatrix} \cos(\theta) \\ \sin(\theta) e^{i\chi} \end{pmatrix}^\dagger \begin{pmatrix} 0 & 1 \\ 1 & 0 \end{pmatrix} \begin{pmatrix} \cos(\theta) \\ \sin(\theta) e^{i\chi} \end{pmatrix} = \cos(\theta) \sin(\theta) (e^{i\chi} + e^{-i\chi}) = 0 \tag{3.5}$$

From this I see that the complex phase χ must be $\frac{\pi}{2}$. I thus have one less parameter and my subspace of self-adjoint wavefunctions is parametrized by a single parameter and includes only a single wavefunction. It becomes clear that in this case there was no other choice in equation 3.3 than two wavefunctions that were the same at the surface.

$$H_\theta = \left\{ \psi = \begin{pmatrix} \cos(\theta) \\ i \sin(\theta) \end{pmatrix} \right\} \tag{3.6}$$

3.1 Probability current density for Weyl Hamiltonian

It is interesting, useful and correct that the space of wavefunctions is reduced by a boundary inserted into the system, but what does this reduction of self-adjoint space physically mean? By calculating the current density of the system, I wish to showcase the physical implication of this reduction of the Hilbert space.

$$\frac{d\rho}{dt} = -\nabla \cdot \vec{J} = \frac{d}{dt} (\psi^\dagger \psi) = \frac{d\psi^\dagger}{dt} \psi + \psi^\dagger \frac{d\psi}{dt} \quad (3.7)$$

I find the differentials with regard to time by looking to the time dependent Schrödinger equation with units of $\hbar = 1$.

$$i \frac{d\psi}{dt} = H\psi \Leftrightarrow \frac{d\psi}{dt} = -iH\psi \quad (3.8)$$

$$\frac{d\psi^\dagger}{dt} = i(H\psi)^\dagger \quad (3.9)$$

Substituting and calculating explicitly I find the current. Replacing $k_j = -i\partial_j$

$$\begin{aligned} \frac{d\rho}{dt} &= \sum_{j=x,y,z} i(H_j\psi)^\dagger \psi - i\psi^\dagger (H_j\psi) = \sum_{j=x,y,z} i(-i\partial_j\sigma_j\psi)^\dagger \psi - i\psi^\dagger (-i\partial_j\sigma_j\psi) \\ &= \sum_{j=x,y,z} -(\partial_j\psi)^\dagger \sigma_j\psi - \psi^\dagger \sigma_j (\partial_j\psi) = \sum_{j=x,y,z} -\partial_j (\psi^\dagger \sigma_j \psi) = -\nabla \cdot \vec{J} \end{aligned} \quad (3.10)$$

Making the current:

$$J_j = (\psi^\dagger \sigma_j \psi) \quad (3.11)$$

This was the same equation that had to be 0 at the surface of our system for self-adjointness. We see then that requiring self-adjointness in the system is the same as requiring no probability current to flow out of the system.

4 Boundary condition in linearized TPC

I now turn to the more complicated TPC, derived in section 2. Requiring self adjointness in a system where the wave equation is 0 when $x < 0$ but not restrained in the y and z direction.

$$\langle H\psi|\phi\rangle = \langle\psi|H\phi\rangle \quad (4.1)$$

By integrating by parts, I can make everything simplify except the surface term in the x direction. It is done as following:

$$\begin{aligned} &\int_0^\infty dx \int_{-\infty}^\infty dy \int_{-\infty}^\infty dz \left(-J \begin{pmatrix} 0 & \partial_x & -\partial_z \\ -\partial_x & 0 & -\partial_y \\ \partial_z & \partial_y & 0 \end{pmatrix} \begin{pmatrix} \psi_1 \\ \psi_2 \\ \psi_3 \end{pmatrix} \right)^\dagger \begin{pmatrix} \phi_1 \\ \phi_2 \\ \phi_3 \end{pmatrix} = \\ &\int_0^\infty dx \int_{-\infty}^\infty dy \int_{-\infty}^\infty dz \left(-J \begin{pmatrix} \psi_1 \\ \psi_2 \\ \psi_3 \end{pmatrix} \right)^\dagger \begin{pmatrix} 0 & \partial_x & -\partial_z \\ -\partial_x & 0 & -\partial_y \\ \partial_z & \partial_y & 0 \end{pmatrix} \begin{pmatrix} \phi_1 \\ \phi_2 \\ \phi_3 \end{pmatrix} \end{aligned}$$

$-J$ cancels out on each side of the equation and I suppress the integrals of y and z .

$$\begin{aligned} & \iint \int_0^\infty dx \left(\begin{pmatrix} 0 & \partial_x & -\partial_z \\ -\partial_x & 0 & -\partial_y \\ \partial_z & \partial_y & 0 \end{pmatrix} \begin{pmatrix} \psi_1 \\ \psi_2 \\ \psi_3 \end{pmatrix} \right)^\dagger \begin{pmatrix} \phi_1 \\ \phi_2 \\ \phi_3 \end{pmatrix} \\ &= \iint \int_0^\infty dx \begin{pmatrix} \psi_1 \\ \psi_2 \\ \psi_3 \end{pmatrix}^\dagger \begin{pmatrix} 0 & \partial_x & -\partial_z \\ -\partial_x & 0 & -\partial_y \\ \partial_z & \partial_y & 0 \end{pmatrix} \begin{pmatrix} \phi_1 \\ \phi_2 \\ \phi_3 \end{pmatrix} \end{aligned}$$

I move everything to the left side of the equation and explicitly calculate $H\psi$ and $H\phi$. I then calculate the scalar products.

$$\begin{aligned} & \iint \int_0^\infty dx \begin{pmatrix} \partial_x \psi_2 - \partial_z \psi_3 \\ -\partial_x \psi_1 - \partial_y \psi_3 \\ \partial_z \psi_1 + \partial_y \psi_2 \end{pmatrix}^\dagger \begin{pmatrix} \phi_1 \\ \phi_2 \\ \phi_3 \end{pmatrix} - \begin{pmatrix} \psi_1 \\ \psi_2 \\ \psi_3 \end{pmatrix}^\dagger \begin{pmatrix} \partial_x \phi_2 - \partial_z \phi_3 \\ -\partial_x \phi_1 - \partial_y \phi_3 \\ \partial_z \phi_1 + \partial_y \phi_2 \end{pmatrix} = 0 \\ & \Leftrightarrow \\ & \iint \int_0^\infty dx (\partial_x \psi_2^\dagger - \partial_z \psi_3^\dagger) \phi_1 + (-\partial_x \psi_1^\dagger - \partial_y \psi_3^\dagger) \phi_2 + (\partial_z \psi_1^\dagger + \partial_y \psi_2^\dagger) \phi_3 \\ & - (\psi_1^\dagger (\partial_x \phi_2 - \partial_z \phi_3) + \psi_2^\dagger (-\partial_x \phi_1 - \partial_y \phi_3) + \psi_3^\dagger (\partial_z \phi_1 + \partial_y \phi_2)) \end{aligned}$$

Every term with differentials in y and z cancel out when integrating by parts, since the surface term is 0.

$$\iint \int_0^\infty dx (\partial_x \psi_2^\dagger \phi_1 - \partial_x \psi_1^\dagger \phi_2) - (\psi_1^\dagger \partial_x \phi_2 - \psi_2^\dagger \partial_x \phi_1) \quad (4.2)$$

Since there is translational invariance in k_y and k_z , the wavefunction must take the form $\vec{\psi}(x, k_y, k_z) = e^{ik_y} e^{ik_z} \vec{\psi}(x)$. The integrals over y and z can thus be evaluated and I get the following, where k_j and k'_j are the momentum vector in the j direction for the ψ wavefunction and ϕ wavefunction respectively.

$$\delta(k_y - k'_y) \delta(k_z - k'_z) \int_0^\infty dx (\partial_x \psi_2^\dagger \phi_1 - \partial_x \psi_1^\dagger \phi_2) - (\psi_1^\dagger \partial_x \phi_2 - \psi_2^\dagger \partial_x \phi_1) \quad (4.3)$$

Doing integration by parts in regards to x , I can make the rest of the integral cancel out and be left with just our surface term. Suppressing the Dirac delta functions for ease of reading.

$$\int_0^\infty dx (\partial_x \psi_2^\dagger \phi_1 - \partial_x \psi_1^\dagger \phi_2) + (\partial_x \psi_1^\dagger \phi_2 - \partial_x \psi_2^\dagger \phi_1) - [\psi_1^\dagger \phi_2 - \psi_2^\dagger \phi_1]_{x=0}^{x=\infty} = 0$$

$$[\psi_2^\dagger \phi_1 - \psi_1^\dagger \phi_2]_{x=0} = 0 = \langle \psi | Q | \phi \rangle \quad Q = \begin{pmatrix} 0 & -1 & 0 \\ 1 & 0 & 0 \\ 0 & 0 & 0 \end{pmatrix} \quad (4.4)$$

where I suppress the index to evaluate at 0, such that $\psi|_{x=0} = \psi$ and I assume the wavefunction to be 0 at infinity. This is justified by the fact that we are going to look for real exponentially decaying solutions later.

Equation 4.4 constitutes a constraint on the wavefunction spinors. To deduce what space $(D(Q))$ of spinors I have available that makes the Hamiltonian self-adjoint, I start with an arbitrary normalized complex 3-vector and narrow down the scope of it using equation 4.4.

$$\psi_j(x=0) = \begin{pmatrix} \cos(\theta_j) \sin(\phi_j) \\ \sin(\theta_j) \sin(\phi_j) e^{i\varepsilon_j} \\ \cos(\phi_j) e^{i\chi_j} \end{pmatrix} \quad (4.5)$$

An arbitrary normalized 3-vector has 5 degrees of freedom in the form of parameters, one for each dimension in both real and imaginary space, and 1 less because it is normalized. I can add an arbitrary phase to my entire wavefunction, which I use to remove the possibility of the first row being imaginary, reducing the degrees of freedom to 4.

I take two generic wavefunctions ψ_1 and ψ_2 and insert them into equation 4.4.

$$\begin{aligned} 0 &= \langle \psi_1 | Q | \psi_2 \rangle = -\cos(\theta_1) \sin(\phi_1) \sin(\theta_2) \sin(\phi_2) e^{i\varepsilon_2} + \cos(\theta_2) \sin(\phi_2) \sin(\theta_1) \sin(\phi_1) e^{-i\varepsilon_1} \\ &= [-\cos(\theta_1) \sin(\theta_2) e^{i\varepsilon_2} + \cos(\theta_2) \sin(\theta_1) e^{-i\varepsilon_1}] \sin(\phi_1) \sin(\phi_2) \end{aligned} \quad (4.6)$$

Any pair of wavefunctions in a given domain $D(Q)$ must fulfill the previous equation. This includes the case $\psi_1 = \psi_2$. Therefore I am placing no extra restrictions on the parameters by looking at and requiring equation 4.6 where $\psi_1 = \psi_2$.

$$0 = \cos(\theta) \sin(\theta) 2i \sin(\varepsilon) \sin^2(\phi)$$

ε is thus $\pi \cdot n$. $\varepsilon = 0$ and $\varepsilon = \pi$, change the sign of the second row but nothing else. This freedom is already given in the freedom of θ , since $\theta \rightarrow -\theta$ yields a sign in the second row as well. ε can therefore be set to 0 with no loss of generality, reducing the degrees of freedom to 3 parameters. Making our requirement for the domain $D(Q)$:

$$0 = [\cos(\theta_2) \sin(\theta_1) - \cos(\theta_1) \sin(\theta_2)] \sin(\phi_1) \sin(\phi_2)$$

This is only possible if $\theta_1 = \theta_2$, independently of the value of ϕ_1 and ϕ_2 . Given this, the complete set of domains of 3-vectors on which the Hamiltonian is self-adjoint is defined by a single parameter θ .

$$D_\theta(Q) = \left\{ \psi = \begin{pmatrix} \cos(\theta) \sin(\phi) \\ \sin(\theta) \sin(\phi) \\ \cos(\phi) e^{i\chi} \end{pmatrix} \forall (\phi, \chi) \right\} \quad (4.7)$$

This means that whatever solutions we gather from our eigenvalue equation, at the surface it must reduce to a spinor inside one of these domains, fixing θ for the system. the same solution and restricted space applies to the TPC system described in equation 2.21, since there is translational invariance in k_2 and k_3 , and a first order differential in x_1 . This result can be shown using the same method.

5 Deriving surface states

I set up the eigenvalue equation with the linearized Hamiltonian in equation 2.21. Since J is just a general energy rescaling factor, I set it to 1.

$$\begin{pmatrix} 0 & -\partial_{x_1} & \mu^\dagger \\ \partial_{x_1} & 0 & C^\dagger \\ \mu & C & 0 \end{pmatrix} \begin{pmatrix} \alpha(x) \\ \beta(x) \\ \gamma(x) \end{pmatrix} e^{i(k_2 \cdot x_2 + k_3 \cdot x_3)} = E \begin{pmatrix} \alpha(x) \\ \beta(x) \\ \gamma(x) \end{pmatrix} e^{i(k_2 \cdot x_2 + k_3 \cdot x_3)} \quad (5.1)$$

From this I get 3 core equations, that define the eigenstates.

$$-\partial_{x_1}\beta + \mu^\dagger\gamma = E\alpha \quad (5.2)$$

$$\partial_{x_1}\alpha + C^\dagger\gamma = E\beta \quad (5.3)$$

$$\mu\alpha + C\beta = E\gamma \quad (5.4)$$

I isolate α from equation 5.2 and 5.4.

$$\alpha = \frac{-\partial_{x_1}\beta E + C\mu^\dagger\beta}{(E^2 - \mu\mu^\dagger)} \quad (5.5)$$

Inserting α into equation 5.4, I isolate γ . So that I now have α and γ as just functions of β and $\partial_{x_1}\beta$.

$$\gamma = \left(\frac{-\mu}{E^2 - \mu\mu^\dagger} \right) \partial_{x_1}\beta + \frac{C}{E} \left(\frac{\mu\mu^\dagger}{E^2 - \mu\mu^\dagger} + 1 \right) \beta \quad (5.6)$$

Combining equation 5.5, 5.6 and 5.3, I can create a differential equation with only β , as an unknown function, using that $C\mu^\dagger$ is real.

$$\begin{aligned} \partial_{x_1}\alpha + C^\dagger\gamma &= E\beta \\ \Leftrightarrow \\ \partial_{x_1} \left(\frac{-\partial_{x_1}\beta E + C\mu^\dagger\beta}{(E^2 - \mu\mu^\dagger)} \right) + C^\dagger \left(\left(\frac{-\mu}{E^2 - \mu\mu^\dagger} \right) \partial_{x_1}\beta + \frac{C}{E} \left(\frac{\mu\mu^\dagger}{E^2 - \mu\mu^\dagger} + 1 \right) \beta \right) &= E\beta \\ \Leftrightarrow \\ -\partial_{x_1}^2\beta + \left(\frac{C\mu^\dagger}{E} - \frac{C^\dagger\mu}{E} \right) \partial_{x_1}\beta + \left(\frac{CC^\dagger}{E^2} (\mu\mu^\dagger + E^2 - \mu\mu^\dagger) \right) \beta &= (E^2 - \mu\mu^\dagger) \beta \\ \Leftrightarrow \\ -\partial_{x_1}^2\beta + (CC^\dagger + \mu\mu^\dagger - E^2) \beta &= 0 \end{aligned}$$

The solutions to this linear homogeneous second order differential equation are exponentials.

$$\beta = e^{-\eta x_1}$$

Inserting the solution I find η to be the following:

$$\begin{aligned}\eta^2 &= CC^\dagger + \mu\mu^\dagger - E^2 \\ \eta &= \pm\sqrt{CC^\dagger + \mu\mu^\dagger - E^2} \\ &= \pm\sqrt{2(2 + \cos(k_2) + \cos(2k_3 - k_2)) - E^2}\end{aligned}\quad (5.7)$$

Looking for localized states on the $x_1 = 0$ surface we have η positive, while on $x_1 = L$ we have η negative. For $CC^\dagger + \mu\mu^\dagger < E^2$ we get imaginary η and we enter the bulk state.

From equation 5.5 and 5.6 we know that α and γ will also be exponential functions of the form:

$$\psi(x_1) = \begin{pmatrix} \alpha(x_1) \\ \beta(x_1) \\ \gamma(x_1) \end{pmatrix} = \begin{pmatrix} \alpha_0 \\ \beta_0 \\ \gamma_0 \end{pmatrix} e^{-\eta x_1} \quad (5.8)$$

Comparing this to equation 4.7 we can find the values of θ , ϕ and χ , from the parameters of k_2 , k_3 and E .

$$\begin{pmatrix} \alpha_0 \\ \beta_0 \\ \gamma_0 \end{pmatrix} = \begin{pmatrix} \cos(\theta) \sin(\phi) \\ \sin(\theta) \sin(\phi) \\ \cos(\phi) e^{i\chi} \end{pmatrix} \quad (5.9)$$

Taking the ratio between β and α from equation 5.5 I can find θ .

$$\frac{\beta}{\alpha} = \tan(\theta) = \frac{\beta}{\frac{-\partial_{x_1} \beta E + C\mu^\dagger \beta}{(E^2 - \mu\mu^\dagger)}} = \frac{E^2 - \mu\mu^\dagger}{\eta E + C\mu^\dagger} = \frac{E^2 - \mu\mu^\dagger}{\pm E \sqrt{CC^\dagger + \mu\mu^\dagger - E^2} + C\mu^\dagger} \quad (5.10)$$

In terms of k_2 and k_3

$$\tan(\theta) = \frac{E^2 - 2(1 + \cos(2k_3 - k_2))}{\pm E \sqrt{2(2 + \cos(k_2) + \cos(2k_3 - k_2)) - E^2} - 2(\cos(k_3 - k_2) + \cos(k_3))} \quad (5.11)$$

I find that for differing signs of η (and thus different sides of the material that our bound states are localized at) there are differing values of the defining parameter for our boundary condition θ , as one might expect since the boundary is different.

I find ϕ by inserting equation 5.9 into equation 5.4.

$$\begin{aligned}\mu \cos(\theta) \sin(\phi) + C \sin(\theta) \sin(\phi) &= E \cos(\phi) e^{i\chi} \\ \Leftrightarrow \\ \tan(\phi) (\mu \cos(\theta) + C \sin(\theta)) &= E e^{i\chi} \\ \Leftrightarrow \\ \tan(\phi) &= \frac{E e^{i\chi}}{\mu \cos(\theta) + C \sin(\theta)}\end{aligned}$$

By taking the absolute value of this expression I can find ϕ independently of χ .

$$\begin{aligned}\tan(\phi) &= \frac{E}{\sqrt{(\mu \cos(\theta) + C \sin(\theta)) (\mu^\dagger \cos(\theta) + C^\dagger \sin(\theta))}} \\ &= \frac{E}{\sqrt{\mu\mu^\dagger \cos^2(\theta) + CC^\dagger \sin^2(\theta) + 2C\mu^\dagger \sin(\theta) \cos(\theta)}}\end{aligned}\quad (5.12)$$

In terms of the conserved wave numbers k_2 and k_3 of our Brillouin zone.

$\tan(\phi) =$

$$\frac{E}{\sqrt{2 + 2 \cos(2k_3 - k_2) \cos^2(\theta) + 2 \cdot \cos(k_2) \sin^2(\theta) + 4(\cos(k_3 - k_2) + \cos(k_3)) \sin(\theta) \cos(\theta)}} \quad (5.13)$$

χ is derived from the phase we removed

$$\begin{aligned} e^{i\chi} &= \tan(\phi) \frac{\mu \cos(\theta) + C \sin(\theta)}{E} = \frac{\mu \cos(\theta) + C \sin(\theta)}{|\mu \cos(\theta) + C \sin(\theta)|} \\ &= \frac{-\left(e^{-ik_3} + e^{i(k_3 - k_2)}\right) \cos(\theta) + \left(1 + e^{-ik_2}\right) \sin(\theta)}{\sqrt{2 + 2 \cos(2k_3 - k_2) \cos^2(\theta) + 2 \cdot \cos(k_2) \sin^2(\theta) + 4(\cos(k_3 - k_2) + \cos(k_3)) \sin(\theta) \cos(\theta)}} \end{aligned} \quad (5.14)$$

6 BZ Analytics comparison to data using amplitude approach

To investigate to what degree these analytical results are correct I received numerical simulation data by Dr. Fulga of Leibniz Institute for Solid State Materials Research (Dresden). The simulations were tight-binding simulations of a system with the Hamiltonian in equation 2.20, with a finite number of unit cells in the a_1 direction, (either 100 or 200) with no translational invariance broken in a_2 or a_3 , making k_2 and k_3 good quantum numbers by which the surface Brillouin zone is defined (Creating an infinite slab whose plane can be defined by being orthogonal to k_1).

I considered data of the exact diagonalization of the Hamiltonian in the energy regime of 0.4-0.5J, in order to avoid overlap with the flat band. These data show, for which values of the momentum components along the surface of the slab, eigenstates occur, with eigenvalues in the simulated spectrum. On figure 4 these states can be seen plotted in the Brillouin zone defined by k_2 and k_3 .

Along side this I received wavefunction data for 3 wavefunctions at specific points in the Brillouin zone, that also had energies in this regime. These points have been marked on figure 4.

To sort these wavefunctions into surface states and bulk states I used a "position" value created by Dr. Fulga that accompanied the data. This position value is the absolute value of the wavefunction at given k_2 , k_3 and E summed over the first half of the material divided by the absolute value of the wavefunction summed across the entire material.

$$pos = \frac{\sum_{a_1=0}^{a_1=L/2} |\psi(a_1, k_2, k_3, E)|}{\sum_{a_1=0}^{a_1=L} |\psi(a_1, k_2, k_3, E)|}$$

Defining x_1 as the coordinate propagating into the slab, parallel to k_1 .

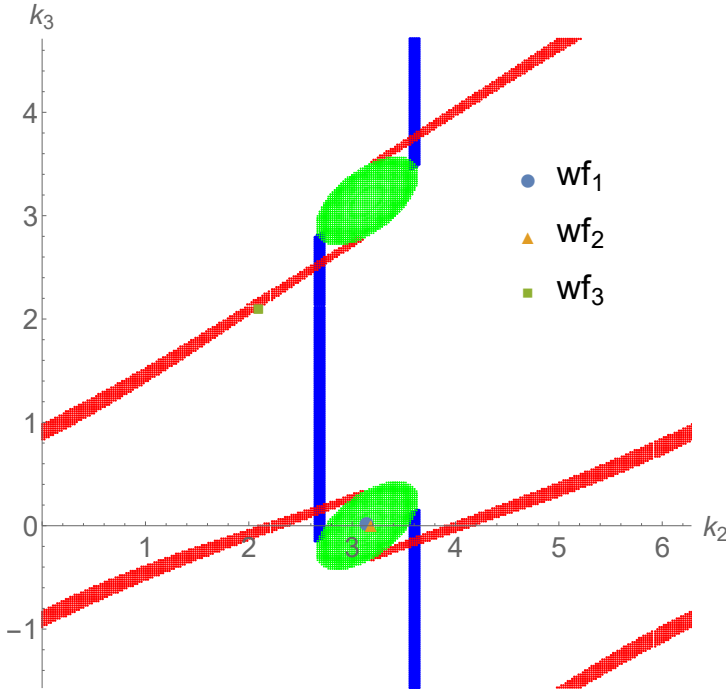


Figure 4: Plot of the Brillouin zone at $E/J = [0.4, 0.5]$ all layered on top of each other. Blue points are states with position in the interval $[0.99, 1]$, red points are states with position in the interval $[0, 0.01]$ and the green points are states with position in the interval $[0.4, 0.6]$. The 3 markers are the 3 surface state wavefunctions I examined. They are dubbed wavefunction 1 through 3. Circle is localized on $x_1 = 0$, triangle is localized on $x_1 = L$ and square is localized on $x_1 = L$, but is strongly localized compared to wavefunction 2.

For surface states we would have a position value that is very close to 0 or 1 depending on whether it is localized on the surface at $x_1 = 0$ or the surface at $x_1 = L$. States far from these position values are not strongly localized. This means that they are either bulk states with imaginary η (see equation 5.7) or localized states with small absolute values of η , resulting in slow exponential decay as a function of system depth from their corresponding surface.

From figure 4 we see green bulk states inside an elongated Fermi surface, projected on the surface Brillouin zone. Two Fermi arcs, one made out of $x_1 = 0$ localized states and one made out of $x_1 = L$ localized states, stretch from the triple point crossing at $(k_2, k_3) = (\pi, \pi)$, to the triple point crossing at $(k_2, k_3) = (\pi, 0)$. These two Fermi arcs can be deduced and expected from the sign in equation 5.10, which predicts two kinds of surface states continuous in the Brillouin zone based on the sign of η in equation 5.7.

From section 4 we know that the surface states are defined by the boundary condition parameter θ , that describes the boundary of the system. To find out what this value of θ is in our numerical data, I use equation 5.10 for the numerical points at the surface of the simulated material.

$$\tan(\theta) = \frac{|\beta(a_1 = 0)|}{|\alpha(a_1 = 0)|} \quad (6.1)$$

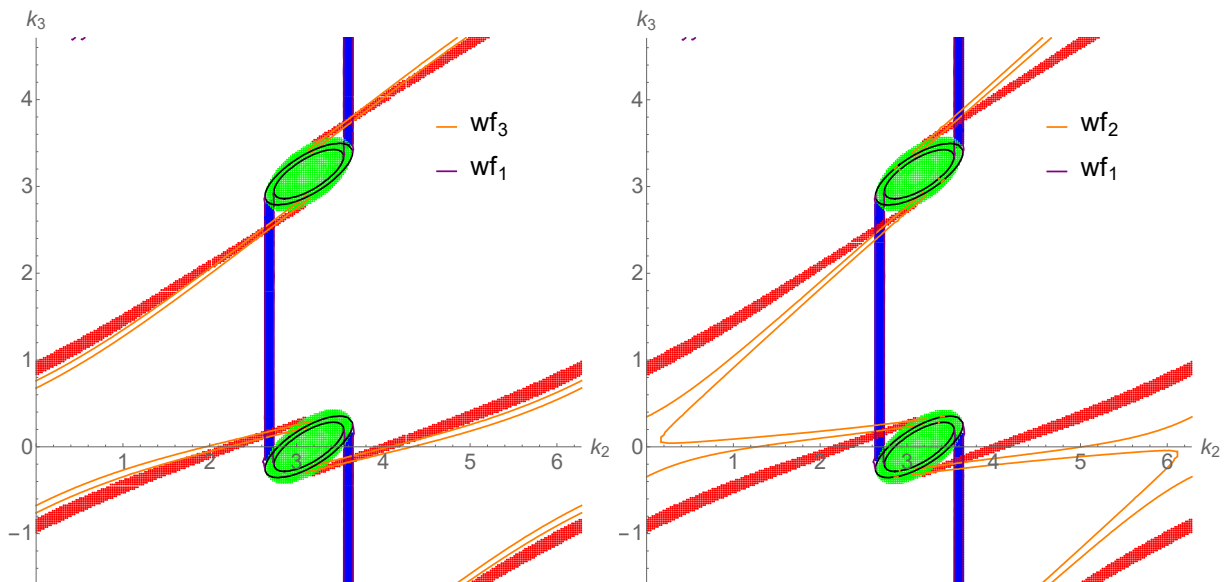


Figure 5: The purple arcs are from wavefunction 1 and match a value of $\theta = \frac{\pi}{2}$ exactly. A state where site 1 has zero amplitude on the surface. The yellow arcs are from wavefunction 3 on the left and wavefunction 2 on the right. Wavefunctions 2 and 3 have negative values of η while 1 has a positive value of η .

By considering the sample wavefunctions with η negative and positive, I can find the two values of θ that define the two Fermi arcs along the two surfaces of the system. I have worked with the data sets of wf1, wf2 and wf3. Wf1 and wf2 are clearly localized, as can be seen on figure 6, but overlap with the bulk states in the Brillouin zone and have very slow exponential decay. Wf3 is very far from the projection of the TPC's and is more strongly localized. On figure 4, the 3 points are marked in the Brillouin zone.

By calculating θ and inserting it into equation 5.11, choosing the sign in equation 5.11 based on which side of the slab the wavefunction is localized on, we get the equation that describe our Fermi arcs in the Brillouin zone for a given energy. This is seen on figure 5, where pairs of them are plotted at energies 0.4J and 0.5J for differing values of θ based on which wavefunction we extracted it from.

7 Analytical wavefunctions compared to data

By calculating η from equation 5.7 and θ from the amplitude approach described in equation 6.1, I obtain wavefunctions from equation 5.8. I compare these analytical functions to the numerical results in figure 6. An important thing to note about these plots is that the wavefunction that is calculated analytically and shown as a solid line, is the exact analytical expression from equation 5.8; there is no fitting parameter. Because η is very important for the normalization of the wavefunction, any change in it will make the plots displaying the absolute value of the wavefunction appear much less accurate. In particular this can be seen on the bottom plots of figure 6, where the logarithmic plot showcases the small difference in η between the data and the analytical function.

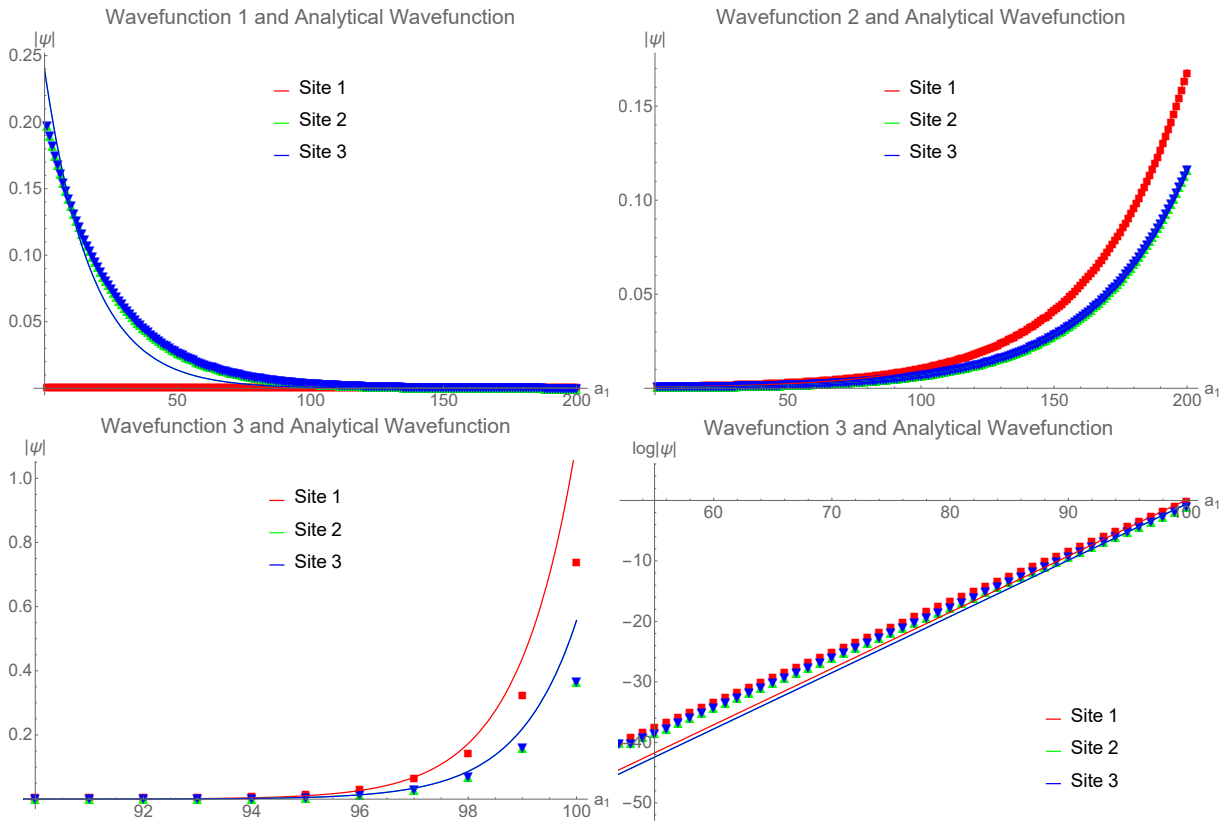


Figure 6: Absolute value of wavefunctions on sites 1 (red), 2 (green), 3 (blue) for wavefunctions 1 through 3. Since 3 is heavily localized a logarithmic plot is also provided.

Another important thing to note is that the x-axes in these plots are measured in the unit cell coordinates a_1 , because the data is sampled for sites in the a_1 direction. This is different from the x_1 coordinate used in my analytics, which is perpendicular to the slabs surface. To remedy this I simply rescale using $x_1 = a_1/\sqrt{2}$. This causes the data and the analytics to sync up in depth into the system perpendicular to the surface, but not in the coordinates along the surface of the system. Since the system is infinite in the k_2 and k_3 direction this has no effect on the absolute value of the wavefunction, but it does mean that the adapted approach, cannot accurately predict the phase of the wavefunction. The linearized approach we use towards k_1 is also unsuitable to estimate this phase, so the loss is minimal.

From looking at this data we see that the amplitudes of site 2 and 3 are the same at the two surfaces, while site 1 has zero amplitude at the $x_1 = 0$ surface. This corresponds to $\theta = \frac{\pi}{2}$ at the $x_1 = 0$ surface and approximately $\theta = 0.15\pi$ at the $x_1 = L$ surface. $\eta \approx 0.057$ in wavefunction 1, $\eta \approx -0.028$ in wavefunction 2 and $\eta \approx -0.940$ in wavefunction 3. Showcasing the expected difference in localization to the surface between the wavefunctions close to the triple point crossing and those far from it.

8 Conclusion

The Weyl semimetal and TPC semimetal systems were studied near the Weyl nodes and TPC, with the goal of finding the maximal reduced Hilbert space $D(Q)$, where the bulk Hamiltonian is self-adjoint after inserting a physical boundary at $x_1 = 0$. It was shown that a boundary could be defined by a single parameter that I dubbed θ . It was shown that this reduction of Hilbert space could physically be understood as restricting probability current from flowing out of the system. A system that hosts TPC's in k -space was derived from a real space Hamiltonian through a Fourier transformation of the fermionic annihilation and creation operators. Utilizing the reduced Hilbert space $D(Q)$ and the preservation of translational invariance in directions x_2 and x_3 , an analytical description was derived for the surface states characteristic of topological semimetals. Using simulation data provided by Dr. Fulga, I found the value for θ based on the relative amplitude of the numerical wavefunctions and compared the analytical description of these wavefunctions to the simulated ones. As seen on figures 5 and 6, the resulting analytics are very close to describing the real phenomenon.

References

- [1] P. A. M. Dirac. The quantum theory of the electron. *DOI: 10.1098/rspa.1928.0023*, 1928.
- [2] H. Weyl. Gravitation and the electron. *Proceedings of the National Academy of Sciences of the United States of America* 15(4), 323, 1929.
- [3] C. Herring. Accidental degeneracy in the energy bands of crystals. *Phys. Rev.* 52, 365, 1937.
- [4] X. Wan, A. M. Turner, A. Vishwanath, and S. Y. Savrasov. Topological semimetal and fermi-arc surface states in the electronic structure of pyrochlore iridates. *Phys. Rev. B* 83, 205101, 2011.
- [5] H.B. Nielsen and M. Ninomiya. A no-go theorem for regularizing chiral fermions. *Physics Letters B, Volume 105, Issue 2-3, p. 219-223*, 1981.
- [6] H.B. Nielsen and M. Ninomiya. The adler-bell-jackiw anomaly and weyl fermions in a crystal. *Phys. Lett. B* 130, 389, 1983.
- [7] N.P. Armitage, E. J. Mele, and A. Vishwanath. Weyl and dirac semimetals in three-dimensional solids. *Rev. Mod. Phys.* 90, 15001, 2018.
- [8] M. Z. Hasan, S. Xu, I. Belopolski, and S. Huang. Discovery of weyl fermion semimetals and topological fermi arc states. *arXiv:1702.07310*, 2017.
- [9] C Chiu, J.C.Y. Teo, A. P. Schnyder, and S. Ryu. Semiclassical dynamics, berry curvature and spiral holonomy in optical quasicrystals. *Rev. Mod. Phys.* 88, 035005, 2016.
- [10] S. Rao. Weyl semi-metals : a short review. *arXiv:1603.02821*, 2016.
- [11] B. Seradjeh and M. Vennettilli. Surface spectra of weyl semimetals through self-adjoint extensions. *Phys. Rev. B* 97, 075132, 2018.
- [12] B. Bradlyn, J. Cano, Z. Wang, M. G. Vergniory, C. Felser, R.J. Cava, and B. A. Bernevig. Beyond dirac and weyl fermions: Unconventional quasiparticles in conventional crystals. *Science* 10.1126/science.aaf5037, 2016.
- [13] I. C. Fulga and A. Stern. Triple point fermions in a minimal symmorphic model. *Phys. Rev. B* 95, 241116(R), 2017.
- [14] I.C. Fulga, L. Fallani, and M. Burrello. Geometrically protected triple-point crossings in an optical lattice. *Phys. Rev. B* 97, 121402, 2018.
- [15] S. Spurrier and N. R. Cooper. Semiclassical dynamics, berry curvature and spiral holonomy in optical quasicrystals. *Phys. Rev. A* 97, 043603, 2018.

-
- [16] Michael Reed and Barry Simon. *Methods of Modern Mathematical Physics, Vol. 2*. Academic Press, 1970.
- [17] L. Lepori, I. C. Fulga, A. Trombettoni, and M. Burrello. Pt invariant weyl semimetals in gauge-symmetric systems. *Phys. Rev. B* *94*, 085107, 2016.
- [18] Y. Hasegawa. Generalized flux states on 3-dimensional lattice. *J. Phys. Soc. Jpn.* *59*, pp. 4384-4393, 1990.
- [19] T. Dubcek, C. J. Kennedy, L. Lu, W. Ketterle, M. Soljacic, and H. Buljan. Weyl points in three-dimensional optical lattices: synthetic magnetic monopoles in momentum space. *Phys. Rev. Lett.* *114*, 225301, 2016.
- [20] B. Andrei Bernevig with Taylor L. Hughes. *Topological Insulator and Topological Superconductors*. Princeton University Press, 1981.

A Appendix

A.1 Berry curvature monopoles of the Weyl Hamiltonian

To give credence to the earlier claim that Weyl nodes are monopoles of Berry curvature, I address the problem of calculating the Berry curvature. The Berry curvature is defined from the Berry connection and the Berry connection is defined as follows [15, 20]:

$$\vec{A} = i \langle \psi | \nabla_k | \psi \rangle \quad (\text{A.1})$$

And the Berry curvature is defined as:

$$\vec{B} = \nabla_k \times \vec{A} \quad (\text{A.2})$$

Where ψ are the eigenstates of the Hamiltonian in question [15]. I therefore start by finding the eigenstates for the Weyl Hamiltonian $\vec{\sigma} \cdot \vec{k}$.

$$H = \vec{\sigma} \cdot \vec{k} = \begin{pmatrix} k_z & k_x - ik_y \\ k_x + ik_y & -k_z \end{pmatrix} \quad (\text{A.3})$$

It is useful to write the Weyl Hamiltonian in spherical coordinates around the Weyl node. Using the following mapping:

$$\begin{aligned} k_x &= k \sin(\theta) \cos(\phi) \\ k_y &= k \sin(\theta) \sin(\phi) \\ k_z &= k \cos(\theta) \end{aligned} \quad (\text{A.4})$$

This yields the Hamiltonian:

$$H = k \begin{pmatrix} \cos(\theta) & \sin(\theta) \cos(\phi) - i \sin(\theta) \sin(\phi) \\ \sin(\theta) \cos(\phi) + i \sin(\theta) \sin(\phi) & -\cos(\theta) \end{pmatrix} \quad (\text{A.5})$$

That has eigenstates:

$$\begin{aligned} \psi_1 &= -e^{-i\phi} \sin\left(\frac{\theta}{2}\right) |1\rangle + \cos\left(\frac{\theta}{2}\right) |2\rangle \\ \psi_2 &= e^{-i\phi} \cos\left(\frac{\theta}{2}\right) |1\rangle + \sin\left(\frac{\theta}{2}\right) |2\rangle \end{aligned} \quad (\text{A.6})$$

With Eigenvalues

$$E = \mp k \quad (\text{A.7})$$

Calculating the Berry connection in spherical coordinates for ψ_1 yields.

$$\begin{aligned} \vec{A} &= i \langle \psi | \nabla_k | \psi \rangle = ie^{i\phi} \sin\left(\frac{\theta}{2}\right) \nabla_k e^{-i\phi} \sin\left(\frac{\theta}{2}\right) + i \cos\left(\frac{\theta}{2}\right) \nabla_k \cos\left(\frac{\theta}{2}\right) \\ &= \frac{i}{2k} \cos\left(\frac{\theta}{2}\right) \cdot \sin\left(\frac{\theta}{2}\right) \hat{\theta} + \frac{1}{k \sin(\theta)} \sin^2\left(\frac{\theta}{2}\right) \hat{\phi} - \frac{i}{2k} \cos\left(\frac{\theta}{2}\right) \sin\left(\frac{\theta}{2}\right) \hat{\theta} \\ &= \frac{1}{k \sin(\theta)} \sin^2\left(\frac{\theta}{2}\right) \hat{\phi} \end{aligned} \quad (\text{A.8})$$

While the Berry curvature is

$$\begin{aligned}
 \vec{B} &= \nabla_k \times \vec{A} = \frac{1}{k \sin(\theta)} \frac{\partial}{\partial \theta} \left(\frac{1}{k \sin(\theta)} \sin^2 \left(\frac{\theta}{2} \right) \cdot \sin(\theta) \right) \hat{k} - \frac{1}{k} \frac{\partial}{\partial k} \left(k \frac{1}{k \sin(\theta)} \sin^2 \left(\frac{\theta}{2} \right) \right) \hat{\theta} \\
 &= \frac{1}{k \sin(\theta)} \frac{\partial}{\partial \theta} \left(\frac{1}{k} \sin^2 \left(\frac{\theta}{2} \right) \right) \hat{k} = \frac{1}{k^2 \sin(\theta)} \cdot \sin \left(\frac{\theta}{2} \right) \cos \left(\frac{\theta}{2} \right) \hat{k} = \frac{1}{2k^2} \hat{k}
 \end{aligned}
 \tag{A.9}$$

Integrating the flux through a sphere around the Weyl node yields the Chern number times 2π .

$$C = \frac{1}{2\pi} 4\pi k^2 \frac{1}{2k^2} = 1
 \tag{A.10}$$